Main-Chain Dynamics of Cardiotoxin II from Taiwan Cobra (*Naja naja atra*) as Studied by Carbon-13 NMR at Natural Abundance: Delineation of the Role of Functionally Important Residues[†]

Chang-Shin Lee,[‡] Thallampuranam Krishnaswamy S. Kumar,[‡] Lu-Yun Lian,[§] Jya-Wei Cheng,[||] and Chin Yu*[,‡]

Department of Chemistry and Department of Life Science, National Tsing Hua University, Hsinchu, Taiwan, ROC and Biological NMR Centre, University of Leicester, United Kingdom

Received August 11, 1997; Revised Manuscript Received October 28, 1997[⊗]

ABSTRACT: Cardiotoxin analogue II (CTX II) is an all β-sheet, small molecular mass (6.8 kDa), basic protein possessing a wide array of biological properties. Nearly complete assignment of the protonated carbon resonances has been achieved by heteronuclear NMR experiments. The study shows that the correlation between the carbon-13 chemical shifts and CTX II structure is good in general, but interesting deviations are also noticed. To characterize the internal dynamics of CTX II, longitudinal, transverse relaxation rates and heteronuclear $^{13}C\{^1H\}$ NOEs were measured for α-carbons at natural abundance by two-dimensional NMR spectroscopy. Relaxation measurements were obtained in a 14.1 T spectrometer for 50 residues, which are evenly spread along the CTX II polypeptide chain. Except for five α-carbons, all data were analyzed from a simple two-parameter spectral density function using the model free approach of Lipari and Szabo. The microdynamical parameters (S^2, τ_e, and R_{ex}) were calculated with an overall rotational correlation time (τ_m) for the protein of 4.8 ns. For most residues, the α-carbons exhibit fast (τ_e < 30 ps) restricted libration motions ($S^2 = 0.79-0.89$). The present study reveals that the functionally important residues located at the tips of the three loops are flexible, and the flexibility of residues in this region could be important in the binding of cardiotoxins to their putative "receptors" which are postulated to be located on the erythrocyte membrane. In addition, the results obtained in the present study support the earlier predictions on the relative role of the lysine residues in the erythrocyte lytic activity of cardiotoxins.

Snake venoms are a mixture of many different toxins of which the neurotoxins (*1*−*3*) and the cardiotoxins (*4*) are the most toxic. Cardiotoxins, isolated from snake venom sources, are single chain, small molecular mass proteins (6.5−7.0 kDa) cross-linked by four disulfide bridges (*5*−*7*). A wide array of biological activities have been reported for this class of proteins (*4*). They are known to cause lysis of erythrocytes, contraction of cardiac muscle, and selective killing (cytotoxic) of certain type of tumor cells (*4*). The exact mode of action of cardiotoxins is still an enigma. To understand the structural basis of the various biological activities of cardiotoxins, we have determined the backbone dynamics of cardiotoxin analogue II (CTX II) isolated from the venom of the Taiwan cobra (*Naja naja atra*). The 3D solution structure of this toxin has already been elucidated using homonuclear ^1H NMR techniques (*8*). The secondary structure of CTX II is shown to be exclusively β-type, consisting of five β-strands protruding from the globular head and three main loops acting as linkers of these β-strands (Figure 1). In this paper, we report the nearly complete assignment of the noncarbonylic, natural abundance ^{13}C NMR resonances of CTX II. We also present analysis of longitudinal relaxation (R_1), transverse relaxation (R_2), and $^{13}C\{^1H\}$ NOEs for most C^α of CTX II, using inverse detected NMR experiments. Although ^{15}N relaxation measurements are routinely carried out to explore the dynamics of a protein (*9*−*14*), the same is not true for ^{13}C relaxation measurements. The measurement of ^{13}C relaxation of isotopically labeled protein samples are accompanied by several difficulties, the major ones being the presence of ^{13}C-^{13}C coupling and contributions from chemical shift anisotropy and dipole−dipole interactions (*15*). Hence, it is advantageous to measure the ^{13}C relaxation at natural abundance; the major drawback, however, is the poor sensitivity. In the case of CTX II, at the time of performing the experiments, isotopically labeled protein is not available. The availability of large amounts of nonrecombinant protein and the fact that this protein is monomeric and stable at high concentrations make ^{13}C relaxation measurements feasible. The ^{13}C relaxation data are interpreted in terms of the so-called model-free approach (*16*), using two to three adjustable parameters for the description of the internal motion.

[†] This work was supported by the National Science Council, Taiwan (NSC 86-2113-M-007-003) and Dr. C. S. Tsou Memorial Medical Research Advancement Foundation (VGHTH-0112) grants.

* Author to whom correspondence should be addressed. Fax: 886-35-711082.

[‡] Department of Chemistry.

[§] University of Leicester.

[||] Department of Life Science.

[⊗] Abstract published in *Advance ACS Abstracts,* December 15, 1997.

S0006-2960(97)01979-X CCC: $15.00
Published on Web 01/06/1998

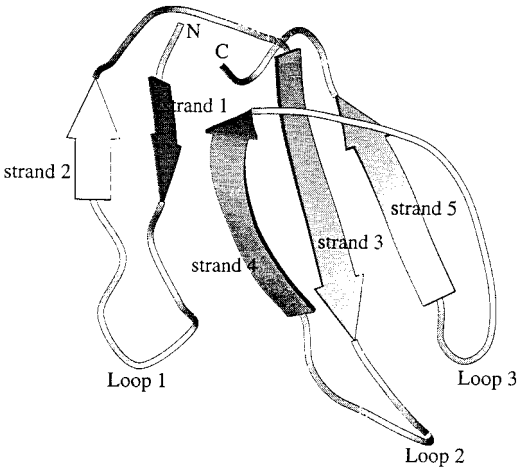

FIGURE 1: Schematic diagram of the three-dimensional structure of CTX II (*8*). The ribbon arrows represent regions of the peptide backbone in β-sheet conformation. The figure was generated using the Program MOLSCRIPT (63).

MATERIALS AND METHODS

Nonrecombinant CTX II was purified as described previously in Bhaskaran *et al.* (*8*). NMR measurements were made by dissolving lyophilized CTX II at pH 3.0 and 298 K. The concentration of the sample used in the experiments was 10 mM. The ^{13}C chemical shifts were referenced to deuterated 3-(trimethylsilyl) propionate, sodium salt (TSP-d_4). All NMR spectra were acquired on Bruker DMX-600 spectrometer equipped with a 5 mm triple resonance probe. The data were processed on a Silicon Graphics INDY workstation using XWIN-NMR software. The ^{13}C chemical shifts were determined by the analysis of HSQC (*17*), HSQC-TOCSY (*18*), and HMBC (*19*) spectra with known ^1H NMR resonances. The secondary chemical shifts ($\Delta\delta$) for C^α and H^α atoms were computed as the difference between observed chemical shifts (δ_{obs}) and the random coil shifts (δ_{rc}) of amino acid residues in water as reported by Thanabal and others (*20*), using the relation,

$$\Delta\delta = \delta_{obs} - \delta_{rc}$$

The secondary chemical shift of each amino acid was plotted against residual number to obtain the chemical shift (CS) plot. The analysis of the CS plot was carried using the method of Wishart and others (*21*).

The pulse sequences used to measure the relaxation parameters for the methine carbons of CTX II are similar to those of Farrow *et al.* (*22*) with suitable modifications to measure carbon-13 relaxation parameters (see Supporting Information Figure S1). For methine carbons, the contribution of chemical shift anisotropy (CSA) to the relaxation is expected to be small (*23*), so experiments have not been modified to suppress cross correlation effects between dipolar interactions and CSA. A Carr−Purcell−Meiboom−Gill (CPMG) spin-echo sequence (*24*, *25*) was applied during the transverse relaxation period, T, of the R_2 experiment. The CPMG sequence minimizes the effects of resonance offset and field nonhomogeneity and suppresses contributions from chemical exchange and scalar relaxation if $k\delta << 1$, where k is the exchange or scalar relaxation rate constant and δ is the CPMG spin-echo time. The water suppression is done by two gradient pulses which are used for coherence transfer, and hence, the water coherence is not selected. Techniques for measuring R_1, R_2, and NOE are the conventional inverse detection and steady state $^{13}C[^1H]$ NOE methods (*26*), respectively. For measurements of R_1 and R_2 rate constants, a recycle delay of 4 s was used between acquisitions to ensure sufficient recovery of ^1H magnetization. R_1 and R_2 experiments were repeated several times using different values of the variable delay times. Nine variable time delays were used for R_1 (0.05, 0.10, 0.20, 0.30, 0.40, 0.60, 0.7, 0.8, and 1.0 s) and eight for R_2 (0.0086, 0.017, 0.0344, 0.043, 0.060, 0.077, 0.094, and 0.140 s) measurements. To calculate $^{13}C\{^1H\}$ NOEs, two spectra were recorded: the first was acquired with broad-band ^1H saturation to achieve NOE enhancement, while the second was acquired without saturation. Three independent pairs of NOE experiments were carried out. In the case of the NOE measurement, a recycle delay of 7.5 s was employed. For NOE measurements, uncertainties in the peak heights were given by the standard deviation of the base-plane noise in the spectra (*27*). The average values of the NOEs and standard errors in the mean were determined from three separate data sets. All spectra were acquired with 432 experiments (2048 data points) with 32 scans, and apodized using a shifted sine bell (90°) function on both dimensions.

Relaxation time coefficients and NOE enhancements were calculated from the intensities, $I(T)$, as a function of the variable delay period, t. For R_1 calculation, $I(T)$ is given by

$$I(T) = I_o \exp(-R_1 t) \quad (1)$$

and for R_2 calculation, $I(T)$ is given by

$$I(T) = I_o \exp(-R_2 t) \quad (2)$$

In eqs 1 and 2, I_o is the initial value for the peak intensity. R_1 and R_2 are the longitudinal and transverse relaxation rates, respectively.

NOEs ($\eta + 1$) are calculated from, $\eta = (I_{sat}/I_{unsat} - 1)$, where I_{sat} and I_{unsat} are intensities corresponding to spectra with and without ^1H saturation, respectively. Since the line shape of each individual resonance is the same for all R_1, R_2, and NOE measurements, intensities can be estimated from the cross-peak heights.

Relaxation of the methine carbon is mainly caused by the reorientation of the heteronuclear C-H vector. The frequency spectrum of this motion is characterized by the spectral density function $J(\omega)$. Assuming that only dipolar and chemical shift anisotropy interactions modulate the local magnetic field at each methine carbon, the longitudinal (T_1^{-1}) and transverse (T_2^{-1}) relaxation rates are given by

$$T_1^{-1} = D_{CH}^2/4[J(\omega_H - \omega_C) + 3J(\omega_C) + 6J(\omega_H + \omega_C)] + CJ(\omega_C)$$

$$T_2^{-1} = D_{CH}^2/8[4J(0) + J(\omega_H - \omega_C) + 3J(\omega_C) + 6J(\omega_H) + 6J(\omega_H + \omega_C)] + C/6[4J(0) + 3J(\omega_C)] + \pi R_{ex}$$

$$NOE = 1 + 4T_1 D_{CH}^2 (\gamma_H/\gamma_C)[6J(\omega_H + \omega_C) - J(\omega_H - \omega_C)]$$

in which,

$$D_{CH} = (h/2\pi)\gamma_C\gamma_H r_{CH}{}^{-3}(\mu_0/4\pi)$$

$$C = (\delta_{//} - \delta_{\perp})^2\omega^2{}_C/3$$

where ω_H and ω_C are the Larmor frequencies for proton and carbon, respectively. μ_0 is the permeability of free space, h is the Planck's constant, δ_C and δ_H are the gyromagnetic ratios of ^{13}C and ^1H, r_{CH} is the carbon-proton bond length (1.09×10^{-10} m), $\delta_{//}$ and $\delta_{\perp}$ are the parallel and perpendicular components of the chemical shift tensor. The difference between $\delta_{//}$ and $\delta_{\perp}$ is set to 25 ppm, a typical value for methine α-carbon nuclei (*28*, *29*). Curve fitting was carried out based on the Levenburg−Marquardt algorithm (*30*) using Sigmaplot software (Jandel Scientific Corp.) to minimize the value of χ^2 goodness of fit parameter (27). Uncertainties in the relaxation were taken to be the standard errors of the fitted parameters. The sufficiencies of the monoexponential decay functions given by eq 1 and 2 were evaluated with a χ^2 test, as described by Palmer *et al.* (1991).

Model free parameters were determined from the relaxation data by using the Modelfree software (version 3.1) (*27*). Parsimonious models for each resonance were selected as described below. An initial estimate for τ_m (the overall correlation time) was obtained from the average R_1/R_2 ratio for the backbone carbon resonances (*27*). A grid search was used to obtain initial guess for the values of the other model free parameters. The optimization minimized the χ^2 function, which is given by

$$\chi^2 = (R_{1i} - R_{1i}{*})^2/R_{1i}{}^2 + (R_{2i} - R_{2i}{*})^2/R_{2i}{}^2 + (\mathrm{NOE}_i - \mathrm{NOE}_i{*})^2/\mathrm{NOE}_i{}^2$$

where, R_{1i}, R_{2i}, and NOE_i are the experimental values of relaxation parameters, R_{1i}*, R_{2i}*, and NOE_i* are the corresponding theoretical values computed for each of the five models outlined in Table 1.

Theoretical values were calculated from the spectral density model for each resonance. Statistical properties of the model free parameters were obtained from the Monte Carlo simulations using 500 randomly distributed synthetic data sets (*31*). The quality of the fit between the experimental data and theoretical model was assessed by comparing the optimal values of Γ_i (the sum-squared error for the ith spin) with the $\alpha = 0.05$ critical value of the distribution of Γ_i determined from the Monte Carlo simulations. The critical value is the value of Γ_i that is exceeded by the specified fraction of the simulated data. The model selection strategy used extensive Monte Carlo numerical simulations to estimate the probability distributions for statistics characterizing the goodness-of-fit between the dynamical models and the experimental data. For each model 500 randomly distributed synthetic data sets were generated. The "model-free" formalism of Lipari and Szabo (*16*) makes the assumption that the overall and internal motions contribute independently to the reorientational correlation function of C-H vectors, the internal motions occur on a much faster time scale during the global rotation of the molecule. For a spherical molecule with isotropic rotational diffusion, spectral density function $J(\omega)$ is expressed in the following form,

Table 1: Spectral Density Functions Used in Analysis of ^{13}C Relaxation Data

model	spectral density functions	optimized parameters	no. of residues
1	$J(\omega) = 2/5[S^2\tau_m/(1 + (\omega\tau_m)^2)]$	S^2	1
2[a]	$J(\omega) = 2/5[S^2\tau_m/(1 + (\omega\tau_m)^2) + (1 - S^2)\tau_e'/(1 + (\omega\tau_e')^2)]$	S^2, τ_e	6
3	$J(\omega) = 2/5[S^2\tau_m/(1 + (\omega\tau_m)^2)]$ $1/T_{2obs} = 1/T_2 + R_{ex}$	S^2, R_{ex}	5
4	$J(\omega) = 2/5[S^2\tau_m/(1 + (\omega\tau_m)^2) + (1 - S^2)\tau_e'/(1 + (\omega\tau_e')^2)]$	S^2, τ_e, R_{ex}	33
5[b]	$J(\omega) = 2/5[S^2\tau_m/(1 + (\omega\tau_m)^2) + S_f{}^2(1 - S_s{}^2)\tau_s'/1 + (\omega\tau_s')^2)]$	$S_f{}^2$, $S_s{}^2$, τ_s	5

[a] $\tau_e' = \tau_m\tau_e/(\tau_m + \tau_e)$. [b] $\tau_s' = \tau_m\tau_s/(\tau_m + \tau_s)$. $S^2 = S_f{}^2S_s{}^2$.

$$J(\omega) = 2/5\{S^2\tau_m/[1 + (\omega\tau_m)^2] + (1 - S^2)\tau_e'/[1 + (\omega\tau_e')^2]\}$$

with $1/\tau_e' = 1/\tau_m + 1/\tau_e$. S^2 is the order parameter, and it describes the relative amplitude of internal motions and ranges from 0 to 1. τ_e is the effective correlation time and describes the temporal scale of the rapid internal motion. τ_m is the overall rotational correlation time of the protein. It can be estimated from the expression,

$$R_2/R_1 \cong \{2D_{CH}{}^2[(4J'(0) + J'(\omega_H - \omega_C) + 3J'(\omega_C) + 6J'(\omega_H) + 6J'(\omega_H + \omega_C)] + C/6[4J'(0) + 3J'(\omega_C)]\}/\{D_{CH}{}^2[J'(\omega_H - \omega_C) + 3J'(\omega_C) + 6J'(\omega_H + \omega_C)] + CJ'(\omega_C)] \quad (3)$$

in which $J'(\omega_i)$, i = C, H, is a simplified spectral density function given by

$$J'(\omega_i) = S^2\tau_m/(1 + \omega_i\tau_m)^2$$

Equation 3 is independent of S^2. For bond vectors with more complex internal dynamics, an extended form of the model-free spectral density function has been developed to include two different time constants for internal motions,

$$J(\omega) = 2/5\{S^2\tau_m/[1 + (\omega\tau_m)^2] + S_f{}^2(1 - S_s{}^2)\tau_s'/[1 + (\omega\tau_s')^2]\}$$

where, $S^2 = S_f{}^2S_s{}^2$. $S_f{}^2$ and $S_s{}^2$ are the order parameters for the fast (picosecond time scale) and slow (nanosecond time scale) internal motions, respectively. τ_s' is the effective internal correlation time for the slow motions (with $1/\tau_s' = 1/\tau_m + 1/\tau_s$).

RESULTS

The ^{13}C Resonances Assignment. The knowledge of proton chemical shifts was sufficient to assign almost all of the ^{13}C resonances from inversed correlation experiments such as HSQC (*17*), HSQC-TOCSY (*18*), and HMBC (*19*). The HSQC spectrum of CTX II showed four demarcated regions, representing the α-carbons, the side chain methylene carbons, the methyl carbons, and the aromatic carbons (Figure 2). The expansion of the region between 70 and 45 ppm (^{13}C) and 6 and 3 ppm (^1H) of the HSQC spectrum showed around 44 signals originating from the α-carbons (Figure 3). The remaining 16 C^{α} resonances could not be assigned unambiguously because of resonance overlap on

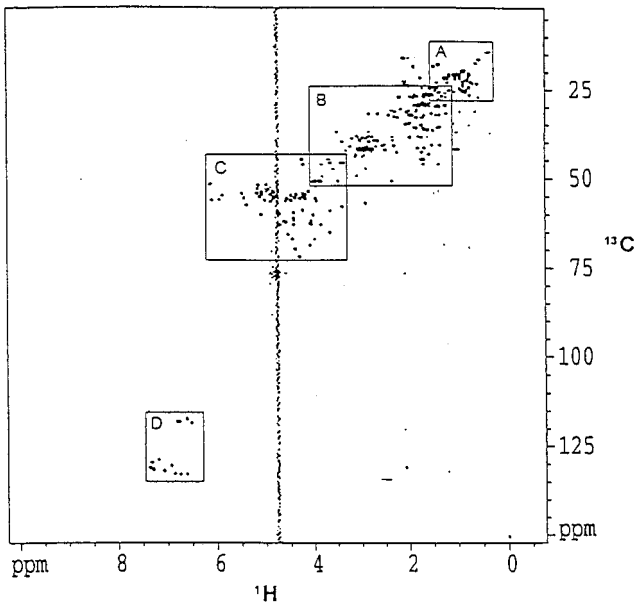

FIGURE 2: HSQC spectrum of CTX II. The frames in the spectrum are the four main regions of ^{13}C NMR resonances classified in the text. (Frame A) Methyl carbons region; (frame B) nonterminal carbons region; (frame C) α-carbons region; (frame D) aromatic region.

^{1}H dimension. However, most of the problems arising from resonances' degeneracy along the ^{1}H dimension in the HSQC spectrum were solved by HMBC and HSQC-TOCSY experiments. The H$^{\alpha}$ chemical shifts of Pro8, Lys35, Leu48, and Val54 were closely overlapped in the range of 4.60−4.62 ppm. Pro8 was distinguished using the characteristic ^{13}C chemical shifts which are 7 ppm downfield shifted (*32*) from the C$^{\alpha}$ resonance frequencies of Leu48 and Val52. Val52 was identified using the HMBC spectrum, and Leu48 was assigned from HSQC-TOCSY data. The assignment of the side chain methylene and the methyl carbons was mostly straightforward. Similarly, certain degree of ambiguity was encountered in some of the methyl groups assignment due to overlap of resonances on the proton dimension. In all these cases, the HMBC and HSQC-TOCSY spectra proved extremely useful in overcoming these ambiguities. There are only five aromatic residues in CTX II (Phe10, Phe25, Tyr11, Tyr22, and Tyr51). As the number of cross-peaks are relatively small in aromatic region (115−140 ppm) of the HSQC spectrum, all the aromatic carbon resonances could be assigned directly.

Cardiotoxin II, is composed of 60 amino acids, including two glycine residues (*8*). The resolution of the spectra was sufficient to obtain the C$^{\alpha}$ relaxation data for 50 out of 58 non-glycine residues evenly spread along the polypeptide backbone. Relaxation data for the remaining eight residues could not obtained due to partial overlap among cross-peaks.

The time dependence of cross-peak intensities for α-carbons from selected residues in fitting R_1 and R_2 curves is shown in Figure 4. The peak heights of several resonances are plotted against variable delay time t and fitted by nonlinear regression to a two-parameter exponential decay (eq 1). The ^{13}C{^{1}H} NOE were extracted from three independent experiments. To calculate the relaxation rates and the NOE, the cross-peak heights in HSQC spectra were measured.

Figure 5 displays the R_1, R_2, and NOE parameters as a function of the amino acid sequence. There is not much variation *per se* in R_1, R_2, and NOE parameters. For most residues, the R_1 values lie in the range 1.3−1.5 s^{-1}. Although, no R_1 values are higher than 1.66 s^{-1}, several are conspicuously higher than 1.3 s^{-1} (for example, Lys2, Met26, Leu30, and Val32). Most of the residues in the middle loop (residues from Leu30 to Ile39) exhibit R_1 values higher than 1.45 s^{-1}. Barring few exceptions, R_2 values are in the range 18−21 s^{-1}. Some residues exhibit slower R_2 relaxation; these included residues Leu9, Tyr11, Lys18, Met24, Lys44, and Leu48. The NOE values do not appear to vary very significantly along the primary sequence of CTX II. For most residues, the NOEs are in the range 1.15−1.28 (Figure 5). However, a few residues have higher values such as Cys3, Val7, Met26, Leu30, and Val32.

Estimation of the Overall Rotational Correlation Time (τ_m). A standard approach for estimating the overall correlation time, τ_m, consists of using R_2/R_1 ratios corresponding to residues in well-defined secondary structures or, to residues for which relaxation is expected to be predominantly driven by fast internal motions. For CTX II, the R_2/R_1 relaxation data yields a τ_m value equal to 5.0 ± 0.5 ns. The value was fixed to obtain the best fit of the five motional models for each residue. The value of τ_m was then optimized simultaneously with the model-free parameters. This cycle was repeated. The final optimized τ_m value was found to be 4.8 ± 0.06 ns. The τ_m value obtained for CTX II in the present study appears to be marginally greater than that obtained for proteins of similar size determined from ^{15}N relaxation measurements. It is well-known that the overall rotational correlation time (τ_m) of proteins (or biological macromolecules) is influenced by the solvent viscosity (*19*). ^{13}C relaxation measurements at natural abundance are known to be relatively insensitive, and hence, most of the protein dynamics studies using carbon-13 NMR are carried out at high protein concentration(s). The high concentration of protein in these studies results in the increase in solvent viscosity leading to a proportionate increase in the overall correlation time (τ_m) of the protein molecules. Thus, the marginal increase in the τ_m observed for CTX II in the present study could be possibly be due to the high concentration (10 mM) of the protein used. It is generally observed that the τ_m values obtained from ^{13}C relaxation measurements at natural abundance are greater than the corresponding values obtained from relaxation measurements carried out using ^{15}N/^{13}C isotope enriched protein(s) (*13*, *54*, *55*).

Analysis of the Relaxation Data. The relaxation data was analyzed by fitting R_1, R_2, and NOE values for each residue to minimize the target function (χ^2). Wherever appropriate, optimization was carried for other terms involved in internal motion and/or chemical exchange. In total, the data were fitted to five different functions which are listed in Table 1. These functions depict a model-free description of the dynamics of the molecule. The relaxation data of all α-carbons were fitted into as simple model as possible to ensure that the optimized parameters were well determined. The α-carbon relaxation data of 50 out of the 60 residues of CTX II could be fitted using the various models listed in Table 1.

Calculation of the Order Parameter (S^2). We used the isotropic model for the correlation function in deriving the

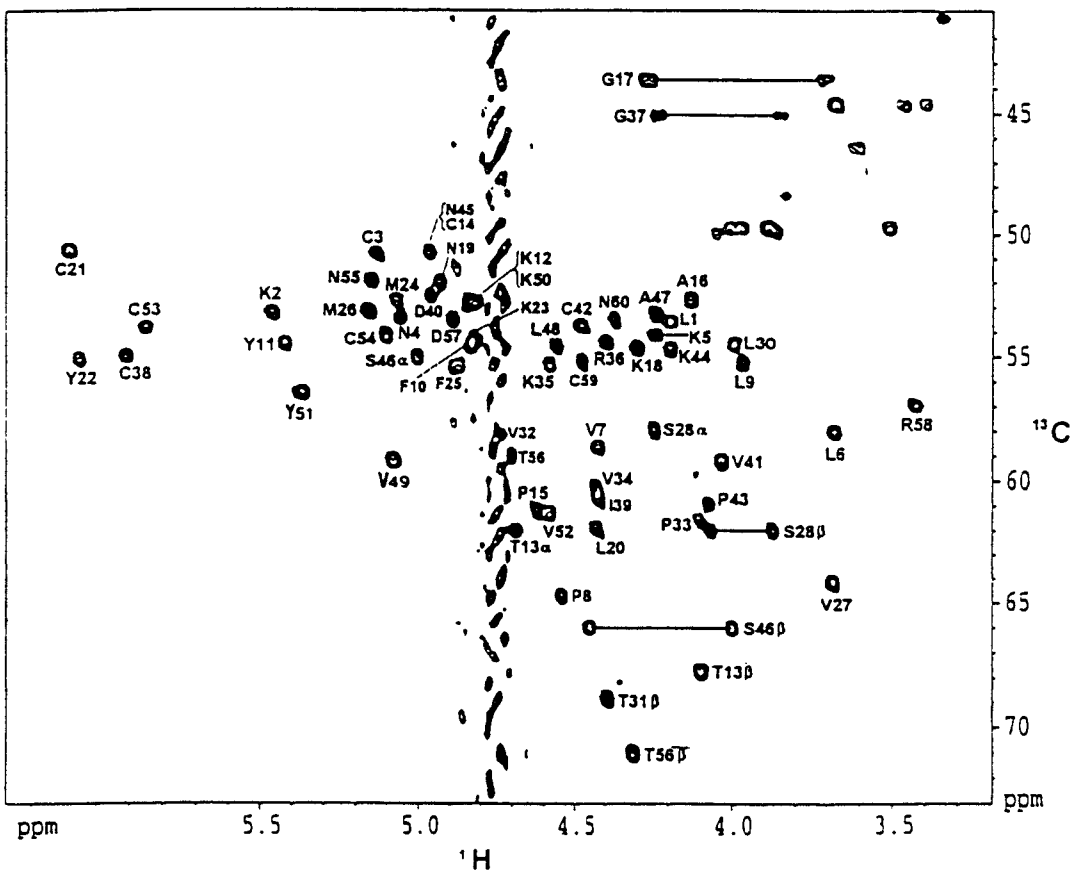

FIGURE 3: C^{α}-H^{α} region (frame C, Figure 2) of the HSQC spectrum of CTX II in 90% H_2O and 10% D_2O at pH 3.0 and 298 K. Sequence-specific assignments of these heteronuclear correlation peaks are designated with one letter code for amino acids and residue number. C^{β}-H^{β} cross-peaks are also shown. For reasons of clarity some cross peaks are not labeled.

Table 2: Average Order Parameter Values for Secondary Structure Elements

structural elements	residues considered	components[a]	totals[a]
N-terminal	1		[1] 0.72
β-sheet			
strand 1	2−4	[3] 0.85	
strand 2	11−13	[2] 0.75	
strand 3	20−25	[5] 0.85	[19] 0.84
strand 4	34−39	[5] 0.89	
strand 5	50−54	[4] 0.80	
loop			
loop 1	5−10	[5] 0.78	
loop 2	26−33	[6] 0.77	[20] 0.78
loop 3	40−49	[9] 0.79	
C-terminal	55−60		[6] 0.76

[a] Number of residues for which data were available is noted in square bracket.

generalized order parameter (S^2). Different procedures may be used for calculating S^2. The order parameter may be calculated exclusively on the basis of the R_1 data, using a single τ_m calculated from the R_2/R_1 ratio of the individual C^{α}. However, this method is known to overestimate the actual order parameter in regions of conformational flexibility. Large random errors are shown to be contained in the S^2 values estimated based on R_1 and NOE values. In the present study, we derive S^2 from a combination of the R_1, R_2, and NOE data, by optimizing the function of S^2 and τ_e. The S^2 and τ_e are plotted in Figure 6. The S^2 values are quite uniform in the secondary structure region and typically fall in the range 0.79−0.89 with the exception of Tyr11 and Tyr51 located in the β-strands spanning residues 11−13 and 50−54, respectively. As shown in Table 2, the flexible regions located in the tip of the three loops of the CTX II

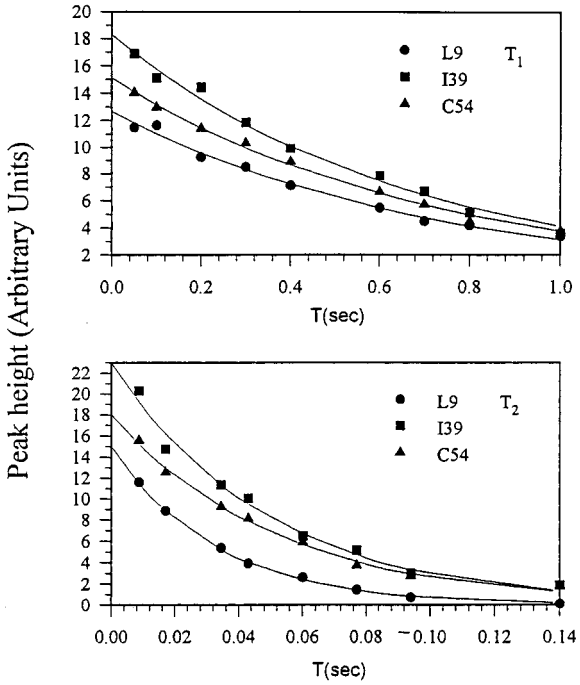

FIGURE 4: Curve fitting of the time dependent experimental R_1 and R_2 values for selected residues of CTX II. T_1-1(R_1) and T_2-1(R_2) are obtained by using a single exponential fit to a decaying function with two parameters using the equation, $I(T) = I_o \exp(-t/T_{1,2})$, where, $I(T)$ is the delay time T and t is the variable delay. I_o is the intensity at zero time.

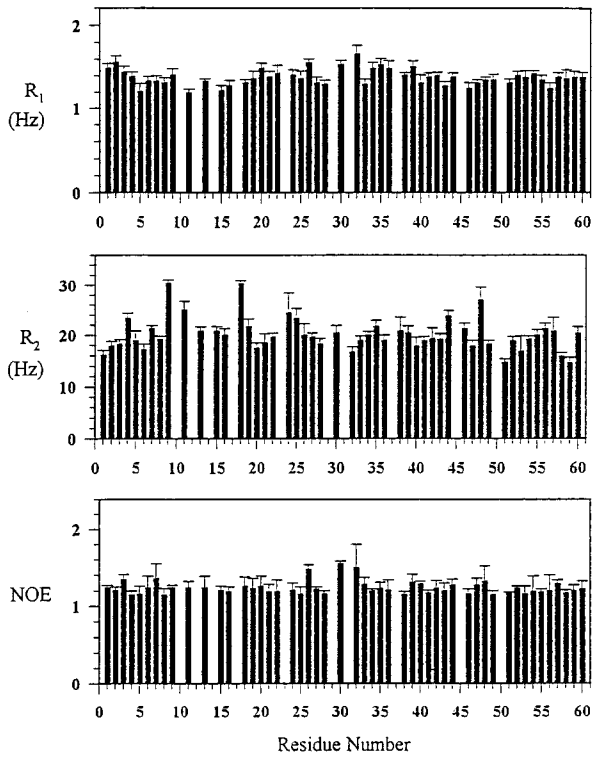

FIGURE 5: Values as a function of residue number of $^{13}C^{\alpha}$ R_1, R_2, and $\{^1H\}^{13}C$ NOEs of CTX II measured at 600 MHz and 298 K. R_1 and R_2 data were obtained by fitting the measured peak heights. NOE values and their uncertainties (indicated by vertical bars) are the average and the standard deviations, respectively, of the values determined from each of three data sets.

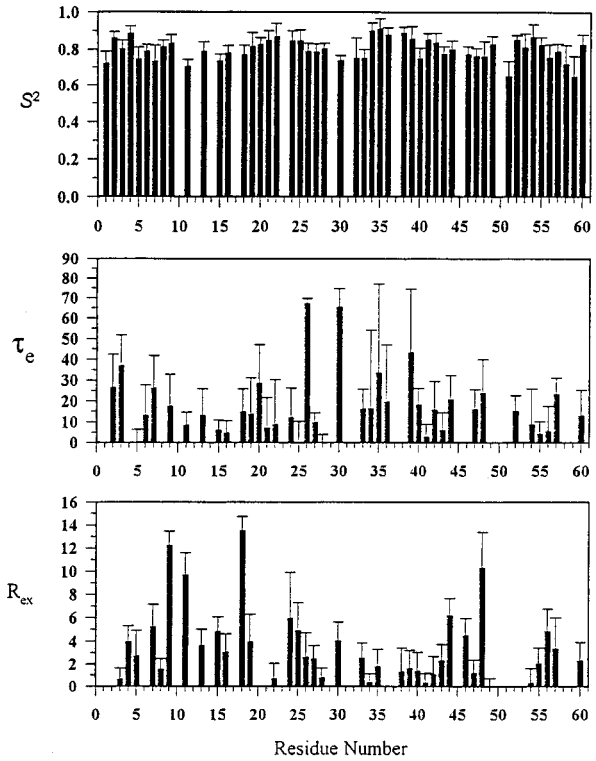

FIGURE 6: Model-free parameter (S^2 and τ_e) and exchange contribution to the transverse relaxation rate (R_{ex}) and uncertainties (indicated by vertical bars) plotted for 50 residues measured. Data were obtained by fitting the relaxation data shown in Figure 5 to the relevant equations according to the criteria discussed in the text.

molecule as expected have lower S^2 values as compared to residues in the β-sheet portions. The S^2 values of residues at the tip of the loops are in the range 0.69−0.79.

DISCUSSION

Conformation-Dependent C^{α} Chemical Shifts. It has been reasonably well established that conformation-dependent chemical shifts of α-carbons can be used to identify regular α-helical and β-sheet conformations in proteins (*35*−*38*). CTX II is composed of three major loops emerging from a globular head. These three loops contain five strands to form double (residues 2−4 and 11−13) and triple (residues, 20−25, 34−39, and 50−55)-stranded antiparallel β-sheets.

Figure 7 displays the secondary shifts ($\Delta\delta$) of the C^{α} and H^{α} atoms *versus* the amino acid sequence of CTX II. It could be seen that the $\Delta\delta C^{\alpha}$ values of amino acid residues between 2−4, 11−13, 20−25, and 50−54 are negative. The negative $\Delta\delta C^{\alpha}$ values, in C^{α} chemical shift (CS) plots, are indicative of these amino acid residues in a β-sheet conformation in the protein (*39*). The negative values appear to correlate well with most of the β-sheet segments in the calculated solution structure of CTX II. Contrary to expectation, the $\Delta\delta C^{\alpha}$ values for the β-sheet segment comprising of residues 35−39 are positive instead of being negative. Interestingly, we found a similar trend in the CS plot of α-carbons of cardiotoxin analogue III isolated from the Taiwan cobra (data not shown). We find this observation intriguing, and at the present juncture, we are unable to offer a concrete explanation for this observed discrepancy. Although good correlation's between experimental $\Delta\delta C^{\alpha}$ values and regular secondary structure of proteins have been reported, the theoretical basis of ^{13}C chemical shifts is/are not completely understood. In addition, it has been reported that ^{13}C chemical shifts are better indicators of α-helix than β-sheet (*40*). It is known that important deviations could arise from local electric fields (like ring current effects of spatially close aromatic side chains or local fields from charged neighbors) (*39*, *41*−*43*) or by the presence of proline residues in the protein segment of interest (*45*−*47*). It is important to mention that the amino acid stretch between residues 34 and 39 contains positively charged amino acids such as lysine at position 35 and arginine at position 36. In addition, there is a proline at position 33 which could contribute to the shielding of amino acid residues which follow them in the amino acid sequence. Interestingly, a β-bulge is consistently found in the three-dimensional structures of all the snake venom cardiotoxins, including CTX II (*8*). This β-bulge is formed by the well conserved proline and valine at positions 33 and 34, respectively. This β-bulge could be classified as a G1-type β-bulge according to the classification of Richardson (*48*). The presence of β-bulge is believed to compensate for the disruption of the regularity of the β-sheet due to the presence of proline at position 33. As normally observed, the β-bulge increases the twist of the three-stranded β-sheet in CTX II (*8*). The twist brought about by the presence of the β-bulge in this region could affect the secondary chemical shift ($\Delta\delta C^{\alpha}$) values of the residues (residues 35−39) involved in the β-strand. In addition, the CS method in some cases fails to identify short sequences of secondary structures (*39*). The reasons mentioned above could be cumulatively or individually responsible for the anomalous behavior of the 34−39 segment in the CS plot of CTX II. The carbon-13 secondary

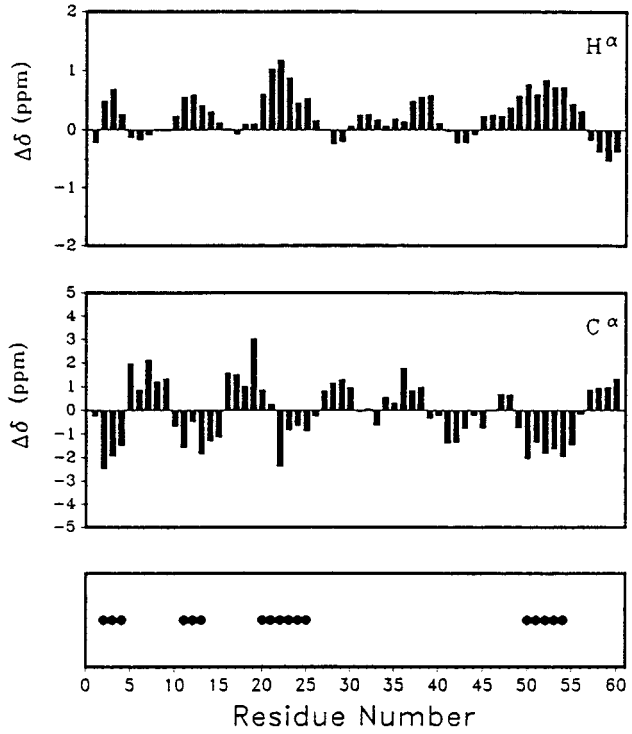

FIGURE 7: Experimental secondary chemical shift plots of H^{α} (top box) and C^{α} (bottom box) atoms of CTX II. Each bar indicates the secondary chemical shift ($\Delta\delta H = \delta_{obs} - \delta_{rc}$) value for each of these atoms in CTX II. The dotted region(s) in the lowermost box indicates the consensus correlation among the H^{α} and C^{α} chemical shift plots and the β-sheet segment(s) in the calculated structure of CTX II. Smoothing of the profile was performed with $n = 1$ (averaging each point with its preceding and following residues). Smoothing of the profile using with various values of n below 1.0 makes no significant change in the profile.

shift values correlated well with most of the β-sheet segments in the structure of CTX II, while similar correlation in the loop region(s) is poor.

Internal Dynamics. Snake venom cardiotoxins show a wide spectrum of biological activities (*4*), but to date, the structure−function relationship of cardiotoxins is poorly understood. Several models have been proposed to explain the variety of biological properties that this class of toxins possess (*4*, *49*−*51*). Chemical modification studies on cardiotoxins have been useful in the identification of residues which are involved in the biological activity (*47*, *51*, *53*). Understanding the main chain internal motions in cardiotoxins could help in correlating the structure of the toxin with its biological activity.

The generalized order parameter (S^2) obtained for the backbone methine carbon in CTX II provides an interesting insight into the relationship between globular protein structure and subnanosecond dynamics. In CTX II, there are five β-strands spanning residues 2−4, 11−13, 20−25, 35−39, and 50−54; these comprise the double- and the triple-stranded antiparallel β-sheet segments in the protein (Figure 1). It can be visualized from Table S1 (Supporting Information), that the five β-strands, as expected, have high S^2 values (0.78−0.87). The β-strands located in the segment of residues 20−25 and 35−39 have higher S^2 values. These β-strands are a part of the triple-stranded β-sheet segment, and they are well conserved in all the cardiotoxin analogues isolated from the venom of the Taiwan cobra. Recently, we characterized a "molten globule"-like protein folding intermediate in the alcohol and acid unfolding pathways (*54*, *55*) of cardiotoxin analogue III (CTX III). The β-strands located between residues 20−25 and 35−39 were found to be intact in the partially structured intermediates characterized along the unfolding pathways of CTX III. Although there is a clear difference in the S^2 values of the residues in the secondary and unstructured regions, the magnitude of difference(s) is not very significant (Table S1). However, similar trends in S^2 values have been reported in the ^{13}C relaxation studies carried out at natural abundance in other proteins (*23*, *33*). Alattia *et al.* (*34*), by studying the internal dynamics of pike parvalbumin, reported that the difference between the S^2 value(s) of residues located in the structured helical segment and the flexible calcium binding loops is unexpectedly very small. Similar observations were made by Farrow *et al.* (*22*), upon studying the dynamics of the *Src* homology domain. In general, the dynamics parameters obtained in this study are similar to those found in other studies of ^{13}C relaxation (at natural abundance) in proteins. More than 50% of the residues in CTX II have very fast internal motions (<20 ps, Figure 8). Since, no clear correlation exists in the relaxation data pertaining to S^2 and τ_e values, we are unable to draw any significant conclusion(s) from the distinctly large τ_e values obtained for the methine carbons of some of the residues. However, it is not uncommon to observe broad correlation between the S^2 and τ_e values. Barbeto *et al.* (*56*), studying the backbone dynamics of calmodulin, observed that lower S^2 values in certain flexible regions of the molecule correlates to higher values of τ_e. However, such a correlation between S^2 and τ_e values was not found in the other portions of the calmodulin molecule. The exchange contribution from the transverse relaxation rate (R_{ex}) is sensitive to the motion on the microsecond to the millisecond time scale if these produce changes in the resonance frequency. R_{ex} values reflect motions slower than the overall tumbling, some of which may be implicated in the biological activity of the protein (*23*). However, as R_{ex} is determined to minimize the difference(s) between experimental and calculated R_2 relaxation rates during the optimization procedures, it is prone to large errors.

The dynamics data obtained in CTX II could be very useful in understanding the flexibility of residues which are implicated in the biological activity of the toxin (*57*). Snake venom cardiotoxins are three finger proteins with three loops projecting from a globular head. Although, the structural basis for the erythrocyte lytic activity of this class of toxins is still not well understood, specific "receptors" are believed to be involved in the selective binding of cardiotoxins (*4*). There are many models proposed describing the interaction of cardiotoxins with the erythrocyte membrane. Dufourcq *et al.* (*58*, *59*), examining the cardiotoxin−lipid interactions, postulated that the hydrophobic residues located at the tip of loop 1 (due to their high flexibility) could constitute the erythrocyte-interaction site of cardiotoxins. They believed that the residues located at the tips of loops 2 and 3 are less flexible and, hence, are not possibly involved in the receptor binding. Batenburg *et al.* (*60*) predicted that the putative receptor binding regions of snake cardiotoxins are spread among the residues located at the tips of all the three loops. These authors contemplate that flexibility of the residues located at the tips of the three loops facilitates the interaction

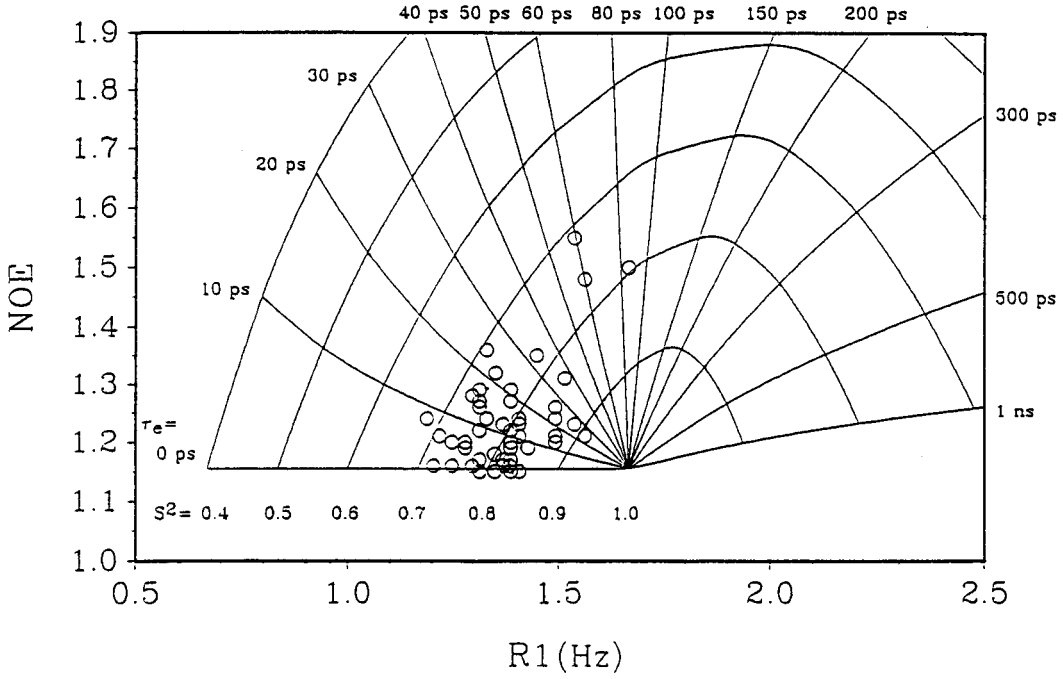

FIGURE 8: Representation of the microdynamical parameters of 50 α-carbon atoms in CTX II in the R_1, NOE plane. Theoretical curves are drawn for different values of τ_e (from 0 to 1 ns) and S^2 (0.4−1). Note that for $S^2 = 1$, all curves reduce to a single point.

of the cardiotoxin molecules with their receptor sites on the erythrocyte membrane. Interestingly, the average order parameter (S^2) values of residues located at the tips of the three loops in CTX II, namely, 5−10 (loop 1), 26−33 (loop 2), and 40−49 (loop 3) are 0.78, 0.77, and 0.79, respectively (Table 2 and Figure 6). Thus, it appears that the residues located at the tip of the loops are relatively more flexible and possibly constitute the multipoint receptor binding sites. The higher flexibility of residues could have significant effect(s) on the thermodynamics and kinetics of ligand receptor binding of cardiotoxins. The rate of association of the toxin to the receptor could have increased, since the high flexibility of the residues located at the tips of the three loops could favor the complex formation with receptor site by lowering the free-energy barrier.

Snake venom cardiotoxins possess three well-conserved tyrosine residues at positions 11, 22, and 51 (*57*). The near-UV CD spectra of cardiotoxins from the Taiwan cobra (*Naja naja atra*) show a broad positive ellipticity CD band centered at around 275 nm. There is still a lot of debate as to which of the three tyrosines in cardiotoxins contributes to the near-UV CD signal (*53*). The near-UV CD signal in proteins is generally believed to stem from the aromatic residues whose aromatic ring(s) have restricted motion because of noncovalent interactions in the three-dimensional structure of this protein. Interestingly, upon comparison of the S^2 values of the α-carbons of the three tyrosine residues in CTX II, it appears that the tyrosine residue located at position 22 ($S^2 = 0.87$) is in a more restricted environment than the other two tyrosine residues situated at positions 11 ($S^2 = 0.70$) and 51 ($S^2 = 0.65$). Thus, it is possible that the restricted motion of the aromatic side chain of tyrosine 22 could be responsible for the near-UV CD signal of snake venom cardiotoxins.

There are two methionine residues at positions 24 and 26. These two methionines are well conserved in all the snake venom cardiotoxins. Nonselective chemical modification of these methionine residues revealed that they are important for the lethal activity of cardiotoxin(s) (*49*). Due to the nonselective nature of the modification reagent used, it is not clear whether one or both of these methionine residues are involved in the toxicity of cardiotoxins. Carlsson and Louw (*49*), studying the role of methionine residues in the lethal activity of cardiotoxin $V^{II}1$ from *Naja melanoleuca*, predicted that the more solvent accessible and flexible methionine residue could be responsible for the lethal action. It can be seen that Met24 and Met26 in CTX II have order parameter values of 0.82 and 0.70 in CTX II, respectively. It appears that Met26 is more flexible than Met24. Thus, based on the suggestion of the earlier workers (*47*, *57*) and the present dynamics data, it is possible that Met26 may have a greater role in the lethal activity of cardiotoxins than Met24.

Snake venom cardiotoxins are shown to cause lysis of erythrocytes. Chemical modification studies showed that lysine residues are intricately involved in the lytic activity (*61*, *62*). Cardiotoxins, in general, possess more than eight lysine residues in their amino acid sequence(s). Menez and co-workers (*49*), working on *Naja nigricollis*, predicted that the lysine residues at positions 5, 12, 18, and 44 could be important for the erythrocyte lytic activity (*51*) of cardiotoxins. Interestingly, our dynamics data suggests that lysine residues at positions 5 ($S^2 = 0.74$), 18 ($S^2 = 0.76$), and 44 ($S^2 = 0.80$) are flexible (Table 2). We are unable to obtain the dynamics data on Lys12 due to spectral overlap in the HSQC spectra. It should be of interest to note that the lysine residues located at positions 2 ($S^2 = 0.86$) and 35 ($S^2 = 0.91$) are comparatively more rigid. Thus, our results support the predictions of Menez *et al.* (*51*) that the well-conserved lysine residues located at positions 5, 18, and 44 could be involved in the binding of the cardiotoxin molecules to the negatively charged centers on the RBC membrane. The greater flexibility or solvent exposure of these lysine residues (lysine 5, 18, and 44) could be an important factor in facilitating these positively charged lysine residues to effectively bind

to the erythrocyte membrane through electrostatic interactions (*62*).

Although, useful information about the structure−function relationship of snake venom cardiotoxins is obtained from the present study of CTX II, it is important to validate some of the conclusions reached through independent site-directed mutagenesis experiments. In this context, we have recently cloned and expressed cardiotoxin analogue (*53*), and we are presently engaged in studying the dynamics of the protein using ^{13}C and ^{15}N isotope enriched sample. Such studies, in our opinion, could provide better correlation between the internal dynamics of cardiotoxins and their biological activity.

ACKNOWLEDGMENT

We would like to sincerely thank Dr. Arthur Palmer for providing us the Modelfree program. We also would like to express our appreciation to Dr. David Craik for helpful discussions. We acknowledge the Regional Instrumentation Center, Hsinchu, Taiwan, for allowing us to use the 600 MHz spectrometer facility.

SUPPORTING INFORMATION AVAILABLE

^{13}C Chemical shift values and dynamics data (order parameter and $\chi 2$) of CTX II (Table S1). Pulse sequences for measurement of the relaxation parameters (Figure S1). HMBC spectrum depicting the methyl group region (Figure S2). HSQC spectra showing the nonterminal side-chain carbon region (Figure S3) and the methyl group region (Figure S4). HSQC-TOCSY spectrum showing the NH-C^{α} crosspeaks (Figure S5). HMBC (Figure S6) and HSQC (Figure S7) depicting the aromatic region (11 pages). Ordering information is given on any currrent masthead page.

REFERENCES

1. Yu, C., Lee, C. S., Chaung, L. C., Shei, Y. R., and Yang, C. C. (1990) *Eur. J. Biochem. 193*, 789−799.
2. Yu, C., Bhaskaran, R., Chang, L. C., and Yu, C. (1993) *Biochemistry 32*, 2131−2136.
3. Peng, S. S., Kumar, T. K. S., Jayaraman, G., Chang, C. C., and Yu, C. (1997) *J. Biol. Chem. 272*, 7817−7823.
4. Kumar, T. K. S., Lee, C. S., and Yu, C. (1996) *Adv. Exp. Med. Biol. 391*, 115−129.
5. Bhaskaran, R., Huang, C. C., Chang, D. K., and Yu, C. (1994) *J. Mol. Biol. 235*, 1291−1301.
6. Bhaskaran, R., Yu, C., and Yang, C. C. (1994) *J. Protein Chem. 13*, 503−504.
7. Yu, C., Bhaskaran, R., and Yang, C. C. (1994) *J. Toxin. Toxicol. Rev. 13*, 291−315.
8. Bhaskaran, R., Huang, C. C., Tsai, Y. C., Jayaraman, G., Chang, D. K., and Yu, C. (1994) *J. Biol. Chem. 269*, 23500−23508.
9. Kay, L. E., Torchia, D. A., and Bax, A. (1989) *Biochemistry 28*, 8972−8979.
10. Kordel, J., Skelton, N. J., Akke, M., Palmer, A. G., III, and Chazin, W. J. (1992) *Biochemistry 31*, 4856−4864.
11. Stone, M., Fairbrother, W. J., Palmer, A. G., III, Reizer, J., Saier, M. H., Jr., and Wright, P. E. (1992) *Biochemistry 31*, 4394−4406.
12. Nicholson, L. K., Kay, L. E., Baisseri, D. M., Arango, J., Young, P. E., Bax, A., and Torchia, D. A. (1992) *Biochemistry 31*, 5253−5260.
13. Cheng, J. W., Lepre, C. A., and Moore, J. M. (1994) *Biochemistry* 33, 4093−4098.
14. Allard, P., Jarvet, J., Ehrenberg, A., and Graslund, A. (1995) *J. Biomol. NMR 5*, 133−146.
15. Ribeiro, A. A., King, R., Restivo, C., and Jardetzky, O. (1980) *J. Am. Chem. Soc. 102*, 4040−4045.
16. Lipari, G., and Szabo. A. (1982) *J. Am. Chem. Soc. 104*, 4546−4559.
17. Bodenhausen, G., and Ruben, D. (1980) *Chem. Phys. Lett. 69*, 185−189.
18. Moy, F. J., Scheraga, H. A., Liu, J. F., Wu, R., and Montelione, G. (1989) *Proc. Natl. Acad. Sci. U.S.A. 86*, 9836−9840.
19. Bax, A., Griffey, R. H., and Hawkins, B. L. (1983) *J. Mag. Reson. 55*, 301−315.
20. Thanabal, V., Omencinsky, D. O., Reily, D. O., and Cody, W. L. (1994) *J. Biomol. NMR 4*, 47−59.
21. Wishart, D. S., Sykes, B. D., and Richards, F. M. (1992) *Biochemistry 31*, 1647−1651.
22. Farrow, N. A., Muhandiram, R., Singer, A. U., Pascal, S. M., Kay, C. M., Gish, C. M., Shoelson, S. E., Pawson, T., Forman-Kay, J. A., and Kay, L. E. (1994*) Biochemistry 33*, 5984−6003.
23. Mispelter, J., Lefevre. C., Adjadj, E., Quiniou, E., and Faraudon, V. (1995) *J. Biomol. NMR 5*, 233−244.
24. Carr, H. Y., and Purcell, E. M. (1954) *Phys. Rev. 3*, 630−639. Carlsson, F. H. H., and Louw, A. J. (1978) *Biochim. Biophys. Acta 534*, 325−329.
25. Meiboom, S., and Gill, D. (1958*) Rev. Sci. Instrum. 29*, 686−709.
26. Noggle, J. H., and Schirmer, R. E. (1971) *The Nuclear Overhausser Effect*: *Chemical Applications*, Academic Press, New York.
27. Palmer, A. G, III, Rance, M., and Wright, P. E. (1991) *J. Am. Chem. Soc. 113*, 4371−4380.
28. Janes, N., Ganapathy, S., and Oldfield, E. (1983) *J. Magn. Reson. 54*, 111−119.
29. Naito, A., and McDowell, C. A. (1983) *J. Chem. Phys. 81*, 4795−4802.
30. Press, W. H., Flannery, B. P., Teukolsky, V., and Vellerlimg, W. T. (1986) *Numerical Recipes*, Cambridge University Press, Cambridge.
31. Mandel, A. M., Akke, M. and Palmer, A. G., III (1995) *J. Mol. Biol. 246*, 144−163.
32. Richarz, R., and Wuthrich, K. (1978) *Biopolymers 17*, 2133−2144.
33. Arvidsson, K., Jarvet, J., Allard, P., and Ehrenberg, A. (1994) *J. Biomol. NMR 4*, 653−662.
34. Alattia, T., Padilla, A., and Cave, A. (1996) *Eur. J. Biochem. 237*, 561−574.
35. Pastore, A., and Saudek, V. (1990) *J. Magn. Reson. 90*, 165−181.
36. Lee, M. S., Palmer, A. G., III, and Wright, P. E. (1992) *J. Biomol. NMR 4*, 171−180.
37. Wishart, D. S., Sykes, B. D., and Richards, F. M. (1991) *J. Mol. Biol. 222*, 311−333.
38. Wishart, D. S., and Sykes, B. D. (1994) *Methods Enzymol. 239*, 363−392.
39. Wishart, D. S., and Sykes, B. D. (1994) *J. Biomol. NMR 4*, 171−180.
40. Luginbuhl, P., Szyperski, T., and Wuthrich, K. (1995) *J. Magn. Reson. 109*, 209−233.
41. Ikura, M., Spera, S., Barbato, G., Kay, L. E., Krinks, M., and Bax, A. (1991) *Biochemistry 30*, 9216−9228.
42. de Dios, A. C., Pearson, J. G., and Oldfield, E. (1993) *J. Am. Chem. Soc. 115*, 9768−9773.
43. de Dios, A. C., Pearson, J. G., and Oldfield, E. (1993) *Science 260*, 1491−1496.
44. Laws, D. D., de Dios, A. C., and Oldfield, E. (1995) *J. Biomol. NMR 3*, 607−612.
45. Howarth, O. W., and Lilley, D. M. J. (1978) *Prog. NMR Spectrosc. 12*, 1−40.
46. Clore, G. M., Driscoll, P. C., Wingfield, P. T., and Gronenborn, A. M. (1990) *Biochemistry 29*, 7387−7388.
47. Clore, G. M., Szabo, A., Bax, A., Kay, L. E., Driscoll, P. C., and Gronenborn, A. M. (1990) *J. Am. Chem Soc. 112*, 4989−4999.

48. Richardson, J. S. *Adv. Protein. Chem*. (1981) *34*, 167−339.
49. Carlsson, F. H. H., and Louw, A. J. (1978) *Biochim. Biophys. Acta 534*, 325−329.
50. Gatineau, E., Toma, F., Montenary-Garestier, T., Takechi, M., Fromageot, P., and Menez, A. (1987) *Biochemistry 14*, 2865−2871.
51. Menez, A., Gatineau, E., Roumestand, C., Harvey, A. L., Mouawad, L., Gilquin, B., and Toma, F. (1990) *Biochemie 72*, 575−588.
52. Chien, K. Y., Haung, W. W., Jean, J. H., and Wu, W. G. (1991) *J. Biol. Chem*. *269*, 14473−14483.
53. Kumar, T. K. S., Yang, P. W., Lin, S. H., Wu, C. Y., Lei, B., Lo, S. J., Tu, S. C., and Yu, C. (1996b) *Biochem. Biophys. Res. Commun*. *219*, 450−457.
54. Kumar, T. K. S., Jayaraman, G., Lee, C. S., Sivaraman, T., Lin, W. Y., and Yu, C. (1995) *Biochem. Biophys. Res. Commun*. *207*, 536−543.
55. Sivaraman, T., Kumar, T. K. S., Jayaraman, G., Han, C., and Yu, C. (1997) *Biochem. J*. *321*, 457−464.
56. Barbeto, G., Ikura, M., Kay, L. E., Pastor, R. W., and Bax, A. (1992) *Biochemistry 31*, 5269−5278.
57. Dufton, M. J., and Hider, R. C. (1991) in *Snake Toxins* (Harvey, A. L., Ed.) pp 259−302, Pergamon Press, New York.
58. Dufourcq, J., Faucon, J. F., Bernard, E., Pezelet, M., Tessir, M., Bougis, Z., Van Rietschuotten, J., Delori, P., and Rochat, H. (1982) *Toxicon 20*, 165−174.
59. Dufourcq, J., and Faucon, J. F. (1978) *Biochemistry 17*, 1170−1175.
60. Batenburg, A. A., Bougis, P. E., Rochat, H., Verkleij, A. J., and Kruijff, D. (1985) *Biochemistry 24*, 7101−7110.
61. Kini, H. R., and Evans, H. J. (1989) *Int. J. Peptide Prot. Res. 4*, 277−286.
62. Rao, C. N., Kumar, T. K. S., and Reddy, R. (1990) in *Recent Advances in Toxinology* (Gopalakrishnakone, K., and Tan, C., Eds.) pp 514−520, Venom and Toxin Res. Group, Singapore.
63. Kraulis, P. (1991) *J. Appl. Crystallogr*. *24*, 946−949.

BI971979C